OPEN ACCESS

Original research

NLRP6 deficiency enhances macrophage-mediated phagocytosis via E-Syt1 to inhibit hepatocellular carcinoma progression

Shuang Li,[1] Yuchen Fu,[2] Xiaodong Jia ,[1] Zherui Liu,[1] Zhenwei Qian,[1] Haoran Zha,[1] Guanglin Lei,[1] Lingxiang Yu,[1] Xinfeng Zhang,[1] Ting Zhang,[3] Tianyi Zhang ,[1] Jie Han,[1] Yuanyuan Shi,[2] Rifaat Safadi,[4] Yinying Lu [1,5]

► Additional supplemental material is published online only. To view, please visit the journal online (https://doi.org/10.1136/gutjnl-2024-334448).

[1]Peking University 302 Clinical Medical School, Peking University, Beijing, Beijing, China
[2]Key Technology Research Center for Cell and Gene Industry, Shenzhen Cell Valley Biopharmaceuticals Co, Ltd, Shen Zhen, Guangdong, China
[3]FlowCytology Laboratory, Beijing Gobroad Boren Hospital, Beijing, Beijing, China
[4]Hadassah Hebrew University Medical Center, Jerusalem, Israel
[5]Center for Synthetic and System Biology, Tsinghua University, Beijing, Beijing, China

Correspondence to
Dr Yinying Lu;
luyinying1973@163.com

Received 29 November 2024
Accepted 3 May 2025

To cite: Li S, Fu Y, Jia X, *et al*. *Gut* Epub ahead of print: [*please include* Day Month Year]. doi:10.1136/gutjnl-2024-334448

ABSTRACT

Background Current treatments with tyrosine kinase inhibitors and immune checkpoint inhibitors have limited efficacy for hepatocellular carcinoma (HCC) due to drug resistance. Emerging therapies such as chimeric antigen receptor T (CAR-T) and macrophage-based cell therapies are promising but need to be improved.

Objectives This study investigates the role of macrophage NOD-like receptor family pyrin domain containing 6 (NLRP6) in HCC progression and its therapeutic potential.

Design Immunofluorescence staining was performed in patient samples. Liver tumour models (autonomous, orthotopic, subcutaneous) were developed, and RNA sequencing, flow cytometry and immunohistochemistry were performed in wild-type, *Nlrp6*$^{-/-}$ mice, and cell-specific Nlrp6 knockout mice. Phagocytosis was assessed using particles or tumour cells. Multiomics, immunoprecipitation mass spectrometry, western blot and co-immunoprecipitation were performed to examine the interaction between NLRP6's PYD domain and E-Syt1's SMP domain.

Results CD68 (a macrophage marker) and NLRP6 expression were detected in patient HCC tissues, and patients with lower macrophage NLRP6 expression had longer survival. Compared with their wild-type mice, *Nlrp6*$^{-/-}$ mice and macrophage cell-specific Nlrp6 knockout mice showed delayed tumour growth. Adoptive transfer of *Nlrp6*$^{-/-}$ macrophages reduced tumour growth in vivo. Macrophages from *Nlrp6*$^{-/-}$ mice were more abundant and exhibited enhanced phagocytosis compared with those from wild-type mice. Co-immunoprecipitation and phagocytosis experiments revealed E-Syt1 promoted phagocytosis, which was negatively regulated by NLRP6 through interaction with its PYD domain.

Conclusions NLRP6 promotes HCC progression by inhibiting macrophage infiltration and suppressing phagocytosis via the interaction between its PYD domain and E-Syt1's SMP domain. Transfer of *Nlrp6*$^{-/-}$ macrophages is a promising therapeutic strategy for reducing HCC tumour growth.

WHAT IS ALREADY KNOWN ON THIS TOPIC

⇒ Current drug therapies for hepatocellular carcinoma (HCC) have limited efficacy due to drug resistance, and while macrophages play a role in tumour progression, the mechanisms underlying this remain unclear.

WHAT THIS STUDY ADDS

⇒ This study demonstrates that NOD-like receptor family pyrin domain containing 6 (NLRP6) inhibits macrophage infiltration and phagocytosis in HCC via E-Syt1, with its absence enhancing these processes and reducing tumour growth.

HOW THIS STUDY MIGHT AFFECT RESEARCH, PRACTICE OR POLICY

⇒ These findings suggest that targeting macrophage NLRP6 could offer a new therapeutic strategy for HCC, potentially influencing future treatment approaches and the development of macrophage-based immunotherapies.

INTRODUCTION

In recent years, with the in-depth knowledge of the tissue structure and immune microenvironment of hepatocellular carcinoma (HCC), immunotherapy has gradually become a research hotspot for HCC treatment.[1] The emergence of immunotherapies such as immune checkpoint inhibitors and adoptive cell therapy has brought light to the treatment of HCC.[2 3] Adoptive immunotherapy is a promising therapeutic approach to target infections, autoimmune diseases and malignancies by infusing in vitro activated and expanded autologous or allogeneic immune effector cells into patients.[4 5] In recent years, cellular immunotherapy has been widely used as a novel therapeutic modality for tumour treatment and has achieved positive clinical results.[6 7]

Given the progress made in chimeric antigen receptor T cells (CAR-T) cell therapy for solid tumours and the potential of chimeric antigen receptor natural killer cells (CAR-NK), there is currently great interest among researchers in developing CAR macrophages (CAR-M) for solid tumour therapy.[8] The main sources of CAR-M cells are peripheral blood mononuclear cells, iPSC and

human monocyte leukaemia cells (THP-1).[9] CAR-M has now been tried for a variety of cancer treatments.[10]

The liver, a highly vascularised organ, is rich in innate immune cells, particularly macrophages.[11] These macrophages, which include monocyte-derived macrophages and tissue-resident macrophages, are instrumental in mediating phagocytosis and exerting cytotoxic effects to control the spread of tumours within the liver.[10 12 13] Therefore, macrophage-targeted cell therapy holds great potential for development in the treatment of HCC. However, macrophage-based therapies still have some limitations, one important issue is the number of cells.[14] Macrophages have a relatively weak proliferative capacity, and patients receiving only a limited number of cells may affect the therapeutic effect.[15] The second issue is the limited phagocytic capacity of macrophages, and enhancing their phagocytic function remains a critical challenge that needs to be addressed.[14 16] To address these challenges, we discovered that NOD-like receptor family pyrin domain containing 6 (NLRP6) deficiency enhances macrophage phagocytosis and promotes their accumulation, thereby boosting tumour-killing effectiveness, and we further elucidated the underlying mechanisms involved.

This study aims to elucidate the role of NLRP6 in promoting HCC progression by inhibiting macrophage infiltration and suppressing phagocytic activity through its interaction with E-Syt1. Our findings demonstrate that the adoptive transfer of NLRP6-deficient (*Nlrp6*$^{-/-}$) macrophages significantly inhibits tumour growth in vivo, providing new insights into potential therapeutic strategies for HCC.

METHOD

The detailed methodology and experimental procedures are provided in the online supplemental materials and online supplemental table 4.

RESULTS

NLRP6 deficiency inhibits the progression of HCC

To investigate whether liver macrophage numbers and NLRP6 expression in macrophages are associated with liver cancer survival. We analysed CD68^{+}macrophages and NLRP6 expression in liver tumour tissues from 29 patients who were treated at Peking University 302 Clinical Medical School between 2016 and 2017. Using the median macrophage count and NLRP6 immunofluorescence integrated optical density as cut-off values, survival analysis showed no correlation between macrophage count and survival but revealed a significant negative correlation between NLRP6 expression in macrophages and survival (figure 1A,B, online supplemental figure 1A). These findings highlight a potential role for NLRP6 in macrophage-mediated liver cancer progression, though its direct influence remains to be determined. To investigate these questions, we analysed bulk RNA sequencing (RNA-seq) data from tumour tissues of 115 patients with HCC (GSE76427), revealing that lower Nlrp6 expression correlated with better overall survival (OS) and recurrence-free survival (figure 1C, online supplemental figure 1B). These results highlight the association of elevated Nlrp6 expression with poor prognosis in tumour tissues.

To determine the role of NLRP6 in the progression of HCC, we established a subcutaneous transplantation model by inoculating Hepa1-6 cells into the axilla of wild-type (WT) and *Nlrp6*$^{-/-}$ mice and monitored tumour growth (figure 1D). The results demonstrated that both tumour volume and weight were significantly greater in the WT group compared with those in the *Nlrp6*$^{-/-}$ group (figure 1E–G).

Subsequently, we used a diethylnitrosamine (DEN)-induced HCC model in both WT and *Nlrp6*$^{-/-}$ mice (figure 1H,I). Our results revealed that NLRP6 significantly promoted HCC development. As illustrated in figure 1J–M and online supplemental figure 2A, WT mice consistently developed more tumours in the liver than *Nlrp6*$^{-/-}$ mice, with a notably higher number of tumour nodules and larger tumour sizes observed in the WT group.

We further extended our studies using a DEN plus CCL4 mouse model, designed to simulate HCC development through fibrosis caused by repeated liver injury (figure 1N,O). Consistent with previous results, the *Nlrp6*$^{-/-}$ group exhibited a significantly lower tumour burden compared with the WT group (figure 1P–S, online supplemental figure 2B).

Recognising that repeated liver injury is not the sole contributor to HCC development[17] we investigated whether NLRP6 deficiency could also inhibit HCC driven by oncogenic mutations. To this end, we injected PX330-P53, C-myc-PT3EF1a and pCMV(CAT)T7-SB100 (online supplemental table 1) used high-density transposon vector (HDTV) to induce HCC in WT and *Nlrp6*$^{-/-}$ mice[18] (figure 1T,U). After 5 weeks, the HDTV model resulted in a 100% tumour formation rate in the WT control group (4/4), while only 25% (1/4) of the *Nlrp6*$^{-/-}$ group developed tumours (online supplemental figure 2C). Additionally, the *Nlrp6*$^{-/-}$ group displayed a significantly reduced maximum diameter and number of liver tumours compared with the WT group (figure 1V–Y).

Across all four models, the deletion of the NLRP6 gene consistently resulted in significant tumour shrinkage or complete tumour regression, underscoring the critical role of NLRP6 in HCC formation.

Deletion of NLRP6 increased macrophage infiltration and phagocytosis

To illustrate the mechanism by which NLRP6 influences HCC progression, RNA-seq was used to compare transcriptional differences in tumour tissues from a subcutaneous transplantation model, where Hepa1-6 cells were inoculated into the axillae of WT and *Nlrp6*$^{-/-}$ mice. The enrichment analysis revealed that the primary differences between the two groups were related to the immune system, particularly the innate immune response (figure 2A,B). We then conducted a gene signature analysis using ImmuCellAI-mouse[19] to evaluate the abundance of various immune cell types based on gene expression profiles (figure 2C). This analysis showed an increased expression of macrophage-related genes in *Nlrp6*$^{-/-}$ tumours (figure 2D).

To better characterise the macrophage subsets involved in NLRP6-mediated effects, we performed double immunofluorescence staining using IBA1 (a pan-macrophage marker) and CLEC4F (a Kupffer cell-specific marker)[20–25] in DEN-induced HCC tissues from WT and *Nlrp6*$^{-/-}$ mice, including both tumour and peritumoural tissues. The results revealed a significant increase in IBA1^{+} CLEC4F^{+} Kupffer cells, IBA1^{+} macrophages in the liver tissue of *Nlrp6*$^{-/-}$ mice, indicating an expansion of resident macrophages in the peritumoural region. IBA1^{+} macrophages infiltrate more in the tumour tissues of Nlrp6$^{-/-}$ mice compared with WT. Notably, these double-positive cells were largely absent from the tumour core, suggesting limited Kupffer cell infiltration into the tumour microenvironment despite their overall increase in the liver (figure 2E). To further investigate the immune mechanisms underlying the reduced tumour burden observed in *Nlrp6*$^{-/-}$ mice, we performed flow cytometry to profile myeloid cell infiltration in the liver tumour

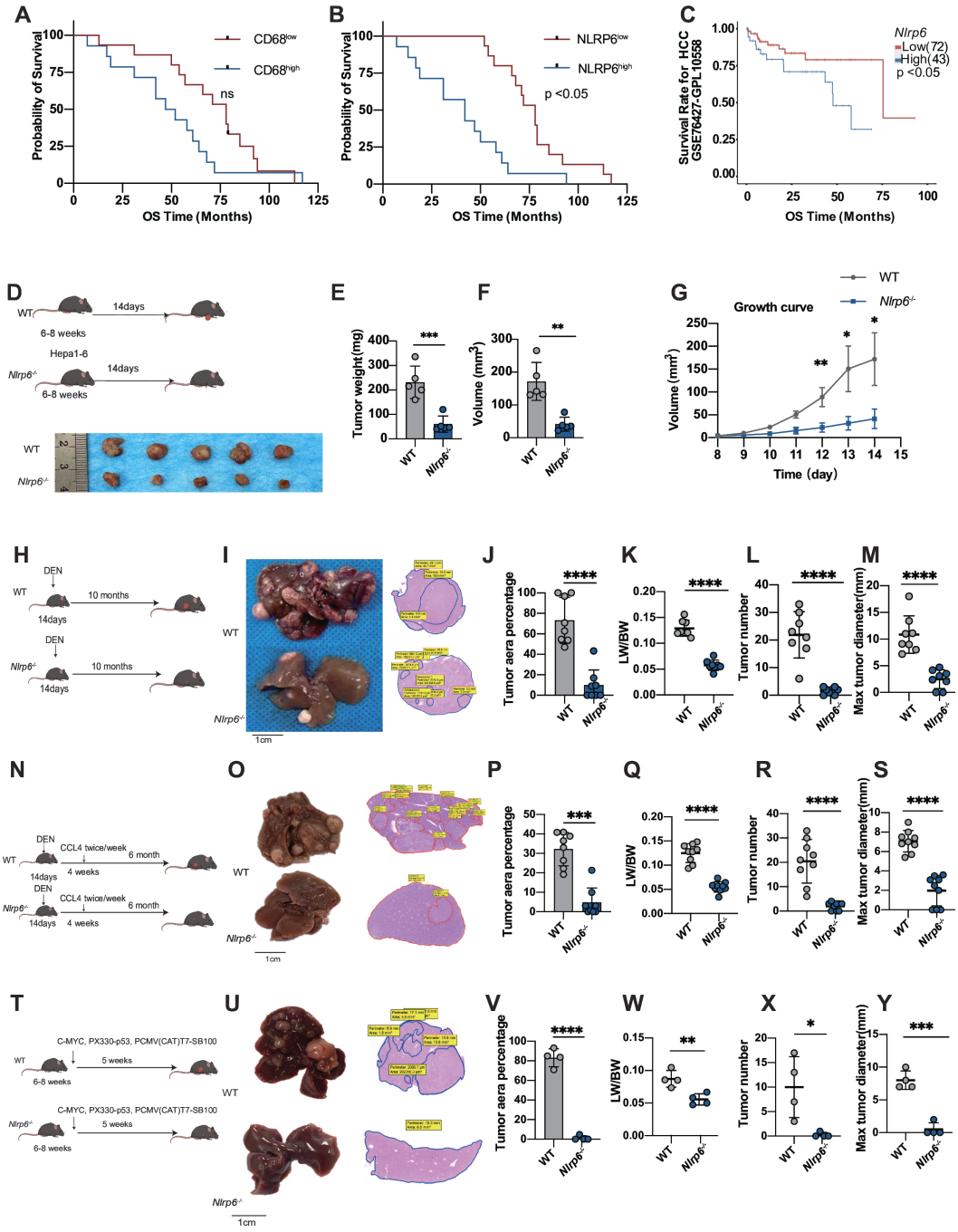

Figure 1 NLRP6 deficiency inhibits HCC proliferation in vivo. (A) The 29 patients were divided into high and low groups based on the median of macrophage count, and overall survival time was compared between the two groups. The log-rank test was used in the overall survival analysis. (B) Using the median NLRP6 immunofluorescence integrated optical density as cut-off values, overall survival time was compared between the two groups. The log-rank test was used in the overall survival analysis. (C) Kaplan-Meier analysis of overall survival (OS) in 115 patients with HCC from the GSE76427 dataset. Patients were categorised into NLRP6 low (n=72) and NLRP6 high (n=43) expression groups based on the optimal cut-off value. (D) Hepa1-6 tumour cells were subcutaneously inoculated into WT and *Nlrp6*$^{-/-}$ mice. Representative images of xenograft tumours derived from Hepa1-6 cells in the two groups of mice. (E) Tumour weight (F) tumour volume (G) tumour growth curves were compared between WT and *Nlrp6*$^{-/-}$ groups. (H–M) Representative images of HCC formation in a DEN-induced HCC mouse model with WT (n=8) or *Nlrp6*$^{-/-}$ (n=8) mice. Hematoxylin and Eosin staining was used to determine the tumour area. Tumour area percentage, liver-to-body weight ratio (L/BW), tumour nodule counts per liver and tumour sizes were quantified and compared. (N–S) Representative images of HCC formation in a DEN plus CCl4-induced HCC model with WT (n=9) and *Nlrp6*$^{-/-}$ (n=9) mice. Tumour area percentage (remove extreme values), L/BW, tumour nodule counts per liver and tumour sizes were quantified and compared. (T–Y) Schematic flow of the hydrodynamic tail vein injection HCC mouse model. Representative images of HCC formation in WT (n=4) and *Nlrp6*$^{-/-}$ (n=4) mice using PX330-P53, C-myc-PT3EF1a, and pCMV(CAT)T7-SB100 at 5 weeks post-injection. Tumour area percentage, L/BW, tumour nodule counts per liver and tumour sizes were quantified and compared. (G) Two-way ANOVA was used. (E, F, J, K, L, M, P, Q, R, S, V, W, X, Y) Unpaired t-test was used. Mean with SD. *p<0.05; **p<0.01; ***p<0.001; ****p<0.0001 from unpaired t-test and two-way ANOVA. ANOVA, analysis of variance; DEN, diethylnitrosamine; HCC, hepatocellular carcinoma; NLRP6, NOD-like receptor family pyrin domain containing 6; WT, wild-type.

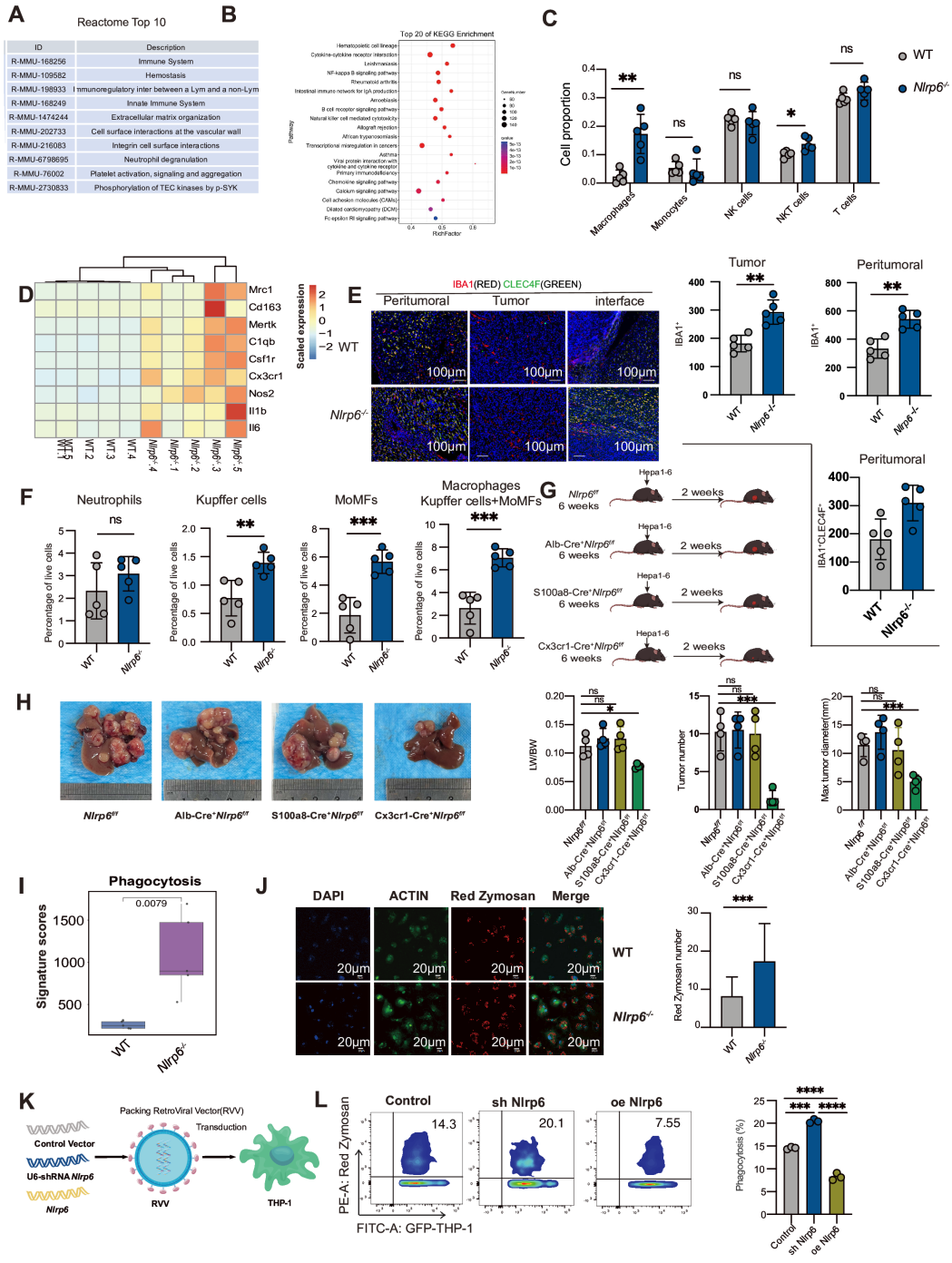

Figure 2 Deletion of NLRP6 increased macrophage infiltration and phagocytosis. (A) Reactome enrichment analysis of differentially-expressed genes (DEGs) from RNA-seq data comparing wild-type (WT) and *Nlrp6*$^{-/-}$ tumours. (B) KEGG (Kyoto Encyclopedia of Genes and Genomes) enrichment analysis of DEGs from RNA-seq data. (C) Primary results of immune cell infiltration analysis using ImmuCellAI-mouse on RNA-seq data, showing changes in immune cell populations between WT and *Nlrp6*$^{-/-}$ groups. (D) Heatmap depicting normalised (z score) values of top DEGs related to macrophage function, showing the differences between WT and *Nlrp6*$^{-/-}$ groups. (E) Immunohistochemical staining of IBA1 (red) and CLEC4F (green) in liver peritumoural and tumour tissue from diethylnitrosamine-induced HCC mouse models of WT and *Nlrp6*$^{-/-}$ mice. (F) Flow cytometry analysis of the number of Kupffer cells, monocyte-derived macrophages, macrophages and neutrophils in liver tumours from *Nlrp6*$^{-/-}$ and WT mice. (G–H) HCC model in conditional knockout mice (n=4 per group). Alb-Cre^{+}*Nlrp6*$^{f/f}$; Cx3cr1-Cre^{+}*Nlrp6*$^{f/f}$ and S100a8-Cre^{+}*Nlrp6*$^{f/f}$, *Nlrp6*$^{f/f}$ mice were injected with Hepa1-6 tumour cells into the portal vein of each mouse group. Liver tumour liver-to-body weight ratio, tumour count per liver and tumour size were compared across groups. (I) Rank sum test showing the enriched phagocytosis-related genes in *Nlrp6*$^{-/-}$ tumours from RNA-seq data. (J) Fluorescence microscopy images showing phagocytic activity in macrophages isolated from liver tissues of WT and *Nlrp6*$^{-/-}$ mice. DAPI (blue): nuclei; ACTIN (green): macrophage morphology; Red Zymosan (red): ingested zymosan particles. Scale bar: 20 μm. (K) Retroviruses were constructed to overexpress or knock down NLRP6 in THP1 cells, with a control vector as reference. (L) Phagocytic activity of THP1 cells (control, shNLRP6 and oeNLRP6) assessed by flow cytometry after co-culture with Red Zymosan. Statistical analyses: (C, E, F, H, J, L) unpaired t-test, mean with SD; significance levels: *p<0.05; **p<0.01; ***p<0.001; ****p<0.0001. HCC, hepatocellular carcinoma; Kyoto Encyclopedia of Genes and Genomes; NLRP6, NOD-like receptor family pyrin domain containing 6; RNA-seq, RNA sequencing; WT, wild-type.

microenvironment. To substantiate this point, we perform flow cytometry to quantify Kupffer ($CD45^+$, $Ly6G^-$, $CD11b^{int}$, $F4/80^+$) and neutrophils ($CD45^+$, $Ly6G^+$, $CD11b^+$, $F4/80^-$), monocyte-derived macrophages (MoMFs) ($CD45^+$, $Ly6G^-$, $CD11b^+$, $F4/80^+$) in the liver tumour microenvironment of WT, *Nlrp6*$^{-/-}$ mice (online supplemental figure 3, figure 2F). The results showed a significant increase in the proportion of infiltrating Kupffer, MoMFs and macrophages in *Nlrp6*$^{-/-}$ mice compared with WT controls, whereas the levels of neutrophils remained unchanged (figure 2F; online supplemental figure 3A–C). To validate these findings histologically, we performed immunofluorescence staining of liver tissue sections using F4/80 (green) and Myeloperoxidase (MPO) (red) to label macrophages and neutrophils, respectively. Consistent with the flow cytometry data, $F4/80^+$ macrophages were markedly increased in *Nlrp6*$^{-/-}$ tumours and peritumoural tissues, while MPO^+ neutrophils showed no significant difference between groups (online supplemental figure 4). Together, these results demonstrate that the enhanced antitumour immunity observed in *Nlrp6*$^{-/-}$ mice is primarily mediated by increased Kupffer cells, MoMFs and macrophage infiltration, rather than by changes in neutrophil populations.

To further determine the cell-type-specific role of NLRP6 in HCC progression, we generated conditional knockout mice by crossing $Nlrp6^{f/f}$ mice (online supplemental figure 5) with Cx3cr1-Cre (macrophage-specific), S100a8-Cre (neutrophil-specific) and Alb-Cre (hepatocyte-specific) strains. To establish an orthotopic liver cancer model, Hepa1-6 tumour cells were injected into the portal vein of each mouse group (figure 2G). Liver tumours were evaluated 2 weeks post-injection. As shown in figure 2H, Cx3cr1-$Cre^+Nlrp6^{f/f}$ mice exhibited the smallest tumour burden, while S100a8-$Cre^+Nlrp6^{f/f}$ and Alb-$Cre^+Nlrp6^{f/f}$ mice showed no significant difference compared with $Nlrp6^{f/f}$ controls. These results indicate that the tumour-suppressive effect observed in Nlrp6-deficient mice is primarily mediated by macrophages, rather than neutrophils or hepatocytes.

We further investigated the regulatory role of NLRP6 on macrophage function by analysing phagocytosis-related gene expression, which was upregulated in the *Nlrp6*$^{-/-}$ group (figure 2I). To confirm whether NLRP6 deficiency enhances macrophage phagocytic function, $CD45^+$ $Ly6G^-$ $CD11b^+$ $F4/80^+$ cells were isolated from the liver tissues of *Nlrp6*$^{-/-}$ and WT mice and co-cultured with Red Zymosan particles in vitro for 2 hours. Microscopic observations and quantification revealed that macrophages from *Nlrp6*$^{-/-}$ mice exhibited significantly augmented phagocytic capacity compared with those from WT mice ($p<0.001$, figure 2J).

To further validate these findings, we constructed a retroviral vector to overexpress or knock down NLRP6 in THP1 cells (online supplemental table 2). Western blot analysis confirmed the transfection efficiency of the retroviral constructs (figure 2K, online supplemental figure 6A). The phagocytic activity of these cells was assessed after co-culture with Red Zymosan. THP1 cells with NLRP6 knockdown showed enhanced phagocytic ability, whereas those overexpressing NLRP6 exhibited diminished phagocytic function (figure 2L). The results demonstrate that NLRP6 negatively regulates macrophage phagocytic function. They demonstrate that NLRP6 negatively regulates macrophage phagocytic function.

Collectively, these findings suggest that NLRP6 promotes HCC progression by inhibiting macrophage infiltration and suppressing their phagocytic function within the liver, while exerting minimal effects on neutrophil recruitment or activity.

Macrophages inhibit HCC via phagocytosis, which is regulated by NLRP6

Our previous findings demonstrated that NLRP6 knockout significantly inhibits the progression of liver cancer by enhancing macrophage function and infiltration. Building on this, we hypothesised that reducing the expression of NLRP6 in macrophages would inhibit HCC through phagocytosis, and that administering these macrophages as a form of cell therapy via intratumoural injection could effectively treat malignant tumours.

To test this hypothesis, we overexpressed and knocked down NLRP6 in THP-1 cells, as mentioned in figure 2, and co-cultured them with RFP-MHCC97H cells. We found that shNLRP6-THP-1 cells enhanced their ability to phagocytose tumour cells (figure 3A).

To evaluate the functional impact of NLRP6-deficient macrophages in vivo, we performed intratumoural injection of bone marrow-derived macrophages (BMDMs) into established tumours in $CD45.1^+$ $C57BL/6J^{Cya\text{-}Ptprcem1(CD45.1)/Cya}$ mice. Tumours were generated using three cancer cell lines—B16F10 (melanoma), MC38 (colon carcinoma) and Hepa1-6 (hepatocellular carcinoma). Beginning on day 4 post-tumour implantation, mice received intratumoural injections of $CD45.2^+$ BMDMs derived from either WT or *Nlrp6*$^{-/-}$ mice, administered every other day for a total of eight injections.

Flow cytometry analysis confirmed successful infiltration of donor-derived macrophages, identified as $CD45.2^+F4/80^+$ cells within the tumour tissue (figure 3C) (online supplemental figure 7). In contrast, control groups (phosphate buffered saline (PBS) mice) showed no $CD45.2^+$ cells, confirming that all $CD45.2^+$ $F4/80^+$ macrophages in the tumours were derived from the injected BMDMs. Mice treated with *Nlrp6*$^{-/-}$ BMDMs exhibited significantly reduced tumour volume and weight compared with those receiving WT BMDMs or PBS, across all three tumour models (figure 3D–F). These findings demonstrate that NLRP6-deficient macrophages have enhanced antitumour capacity, and support the conclusion that NLRP6 suppresses macrophage-mediated tumour immunity in vivo.

These findings suggest that NLRP6 knockdown in macrophages enhances their antitumour activity, leading to more effective tumour suppression. This discovery highlights the potential of NLRP6 as a target for macrophage-based cell therapy, providing a promising new approach to tumour immunotherapy.

NLRP6 and E-Syt1 have a negative feedback regulatory mechanism in cells

To explore the pathway through which Nlrp6$^{-/-}$ inhibits macrophage phagocytosis, we used RNA-seq data from WT and Nlrp6$^{-/-}$ tumour tissues, along with proteomics data from BMDMs and tumour tissues of Nlrp6$^{-/-}$ and WT mice (figure 4A). RNA-seq analysis identified 5135 differentially expressed genes, while proteomics analysis revealed 999 differentially expressed proteins in BMDMs and 812 in tumour tissues. By intersecting these datasets, we identified 69 genes that were both differentially expressed at the transcriptomic and proteomic levels. In addition, immunoprecipitation mass spectrometry using anti-NLRP6 identified 3029 proteins interacting with NLRP6 (figure 4B). Further intersection of the 69 genes with these 3029 interacting proteins narrowed the list to 33 candidate genes. These candidates are involved in pathways potentially regulating macrophage phagocytosis and tumour progression, providing insights into the mechanisms by which NLRP6 influences the tumour microenvironment. A literature

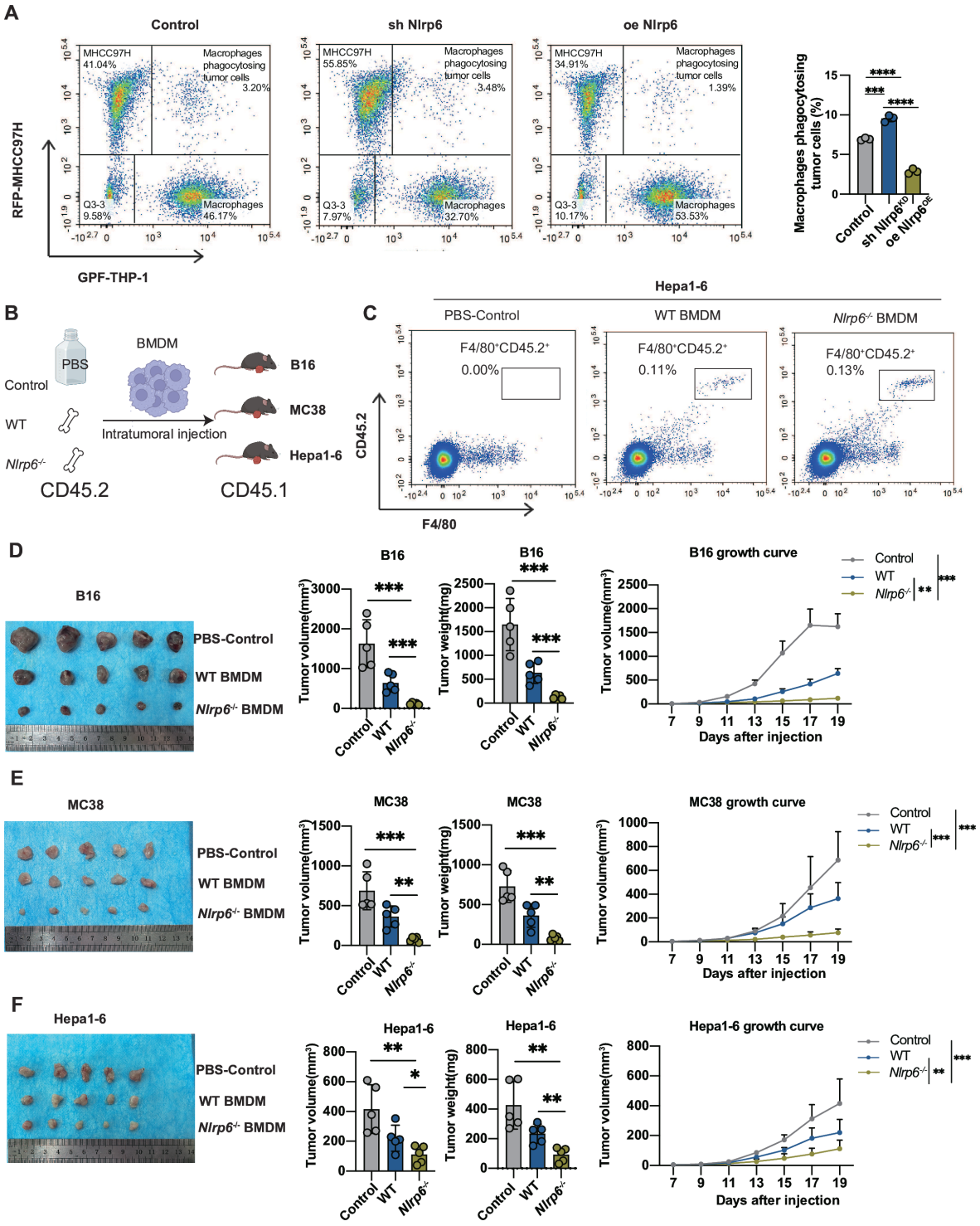

Figure 3 Macrophages inhibit hepatocellular carcinoma via phagocytosis, which is regulated by NLRP6. (A) Flow cytometry based phagocytosis of RFP-MHCC97H tumour cells by control, knocked down and overexpressed NLRP6 in THP-1. Statistical significance was calculated with t-test pairwise comparisons among three groups of data comparisons, and data represent n=3 technical replicates. (B) Schematic showing the procedure of injecting $CD45.2^+$ bone marrow-derived macrophages (BMDMs) into tumours established in $CD45.1^+$ recipient mice ($CD45.1^+$ C57BL/6JCya-Ptprc$^{em1(CD45.1)/Cya}$). The injection was performed to study macrophage infiltration and tumour response in the recipient mice. (C) Representative flow cytometry plots showing the infiltration of donor-derived macrophages ($CD45.2^+$ $F4/80^+$ cells) in Hepa1-6 tumour tissue following injection of PBS, WT BMDMs, or Nlrp6$^{-/-}$ BMDMs. The percentage of $CD45.2^+$ $F4/80^+$ cells in the tumour tissue is indicated for each condition: PBS-control (0.00%), WT BMDM (0.11%) and Nlrp6$^{-/-}$ BMDM (0.13%). (D–F) Tumour tissues from B16F10 (melanoma), MC38 (colon cancer) and Hepa1-6 (liver cancer) xenograft models were analysed. Mice were divided into three groups: PBS control (PBS-control), BMDMs from WT C57BL/6 mice and BMDMs from *Nlrp6*$^{-/-}$ mice. Tumour volume, growth curves and tumour weight were compared across groups. Tumour growth curves were analysed using two-way analysis of variance, and tumour volume and weight comparisons were assessed using an unpaired t-test, mean with SD. Statistical significance is indicated as follows: *p<0.05; **p<0.01; ***p<0.001; ****p<0.0001. PBS, phosphate buffered saline; NLRP6, NOD-like receptor family pyrin domain containing 6; WT, wild-type.

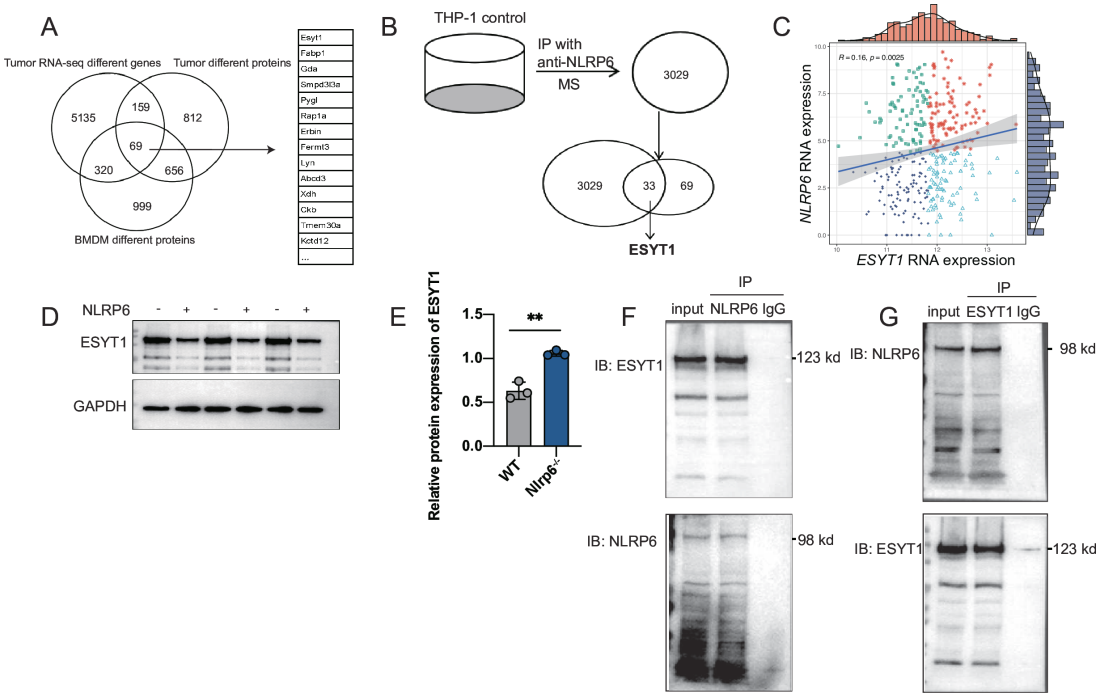

Figure 4 NLRP6 and E-Syt1 have a negative feedback regulatory mechanism within cells. (A) The overlap of differentially expressed genes from WT/*Nlrp6*$^{-/-}$ tumour tissue RNA-seq, BMDM proteomics and liver tumour tissue proteomics. (B) NLRP6 interacting proteins were identified by IP/MS in THP-1 cells. The IP/MS data were further overlapped with Myc-interacting proteins from the UniProt database. (C) This scatter plot shows NLRP6 versus E-Syt1 RNA expression levels across samples in TCGA-LIHC (The Cancer Genome Atlas-Liver Hepatocellular Carcinoma). Points are grouped into four categories based on median expression: high/high (red stars), high/low (green squares), low/high (blue triangles) and low/low (dark blue diamonds). The blue line indicates the linear regression fit. Correlation: R=0.16, p=0.0025. (D) This western blot image shows under NLRP6 knockout ('−') conditions, E-Syt1 expression is higher, while under NLRP6 wild-type ('+') conditions, E-Syt1 expression is lower. GAPDH expression is consistent across all conditions, confirming equal sample loading. (E) Relative protein expression of E-Syt1 from the last western blot. Unpaired t-test was used in the relative expression of E-Syt1. **p<0.01. (F) This image presents the results of a co-immunoprecipitation experiment to investigate the interaction between NLRP6 and E-Syt1. Immunoblot (IB) for E-Syt1. The lanes include input (total cell lysate), immunoprecipitation (IP) with NLRP6 antibody and IgG control. (G) IB for NLRP6. The lanes include input (total cell lysate), IP with E-Syt1 antibody and IgG control. BMDM, bone marrow-derived macrophage; MS, mass spectrometry; NLRP6, NOD-like receptor family pyrin domain containing 6; RNA-seq, RNA sequencing; TCGA-LIHC, The Cancer Genome Atlas-Liver Hepatocellular Carcinoma; WT, wild-type.

review of these genes suggested that E-Syt1 may promote macrophage endocytosis.[26–29] We hypothesise that this molecule could be associated with phagocytic function.

To further validate the relationship between NLRP6 and E-Syt1, we performed a correlation analysis using data from the The Cancer Genome Atlas-Liver Hepatocellular Carcinoma (TCGA-LIHC) database. The correlation coefficient (R) was 0.16, with a p value of 0.0025, indicating a positive correlation between NLRP6 and E-Syt1 expression levels (figure 4C).

Next, we conducted western blot analysis on BMDMs from *Nlrp6*$^{-/-}$ and WT mice. The results showed that the absence of NLRP6 led to an increase in E-Syt1 expression (figure 4D,E). To further explore the interaction between NLRP6 and E-Syt1, we performed a co-immunoprecipitation assay, confirming a specific interaction between these two proteins (figure 4F,G).

E-Syt1 promotes macrophage phagocytosis and its antitumour activity against HCC

Given that phagocytosis is a subtype of endocytosis, we hypothesised that E-Syt1, known for its role in regulating membrane dynamics, may enhance macrophage phagocytic function.[30–32] To test this, we used retroviral vectors to knock down (shE-Syt1) or overexpress (oeE-Syt1) E-Syt1 in THP1 cells (online supplemental table 2) (figure 5A). Western blot analysis confirmed the efficiency of the E-Syt1 knockdown and overexpression constructs in the transfected cells (figure 5B). Next, we assessed phagocytic activity by co-culturing the THP1 cells with Red Zymosan particles and RFP-MHCC97H cells. The results indicated a direct correlation between E-Syt1 expression, phagocytic ability and antitumour activity, suggesting that the antitumour process is based on phagocytosis. Compared with the control group, oeE-Syt1-THP1 cells displayed significantly enhanced phagocytic function, while shE-Syt1-THP1 cells exhibited a marked reduction in phagocytosis (figure 5C,D). These findings suggest that E-Syt1 is critical for enhancing the phagocytic function of macrophages in tumour contexts.

To investigate whether higher expression of E-Syt1 in macrophages correlates with patient outcomes, we analysed liver tumour tissues from 29 patients treated at the Peking University 302 Clinical Medical School between 2016 and 2017. Immunohistochemical staining for CD68 (a macrophage marker) and E-Syt1 revealed that patients with a higher proportion of CD68^{+}/E-Syt1^{+} double-positive cells had significantly improved OS rates compared with those with lower double-positive cell counts (figure 5E,F). These results indicate that E-Syt1 enhances macrophage phagocytosis and that higher E-Syt1 expression in macrophages is associated with better patient survival outcomes.

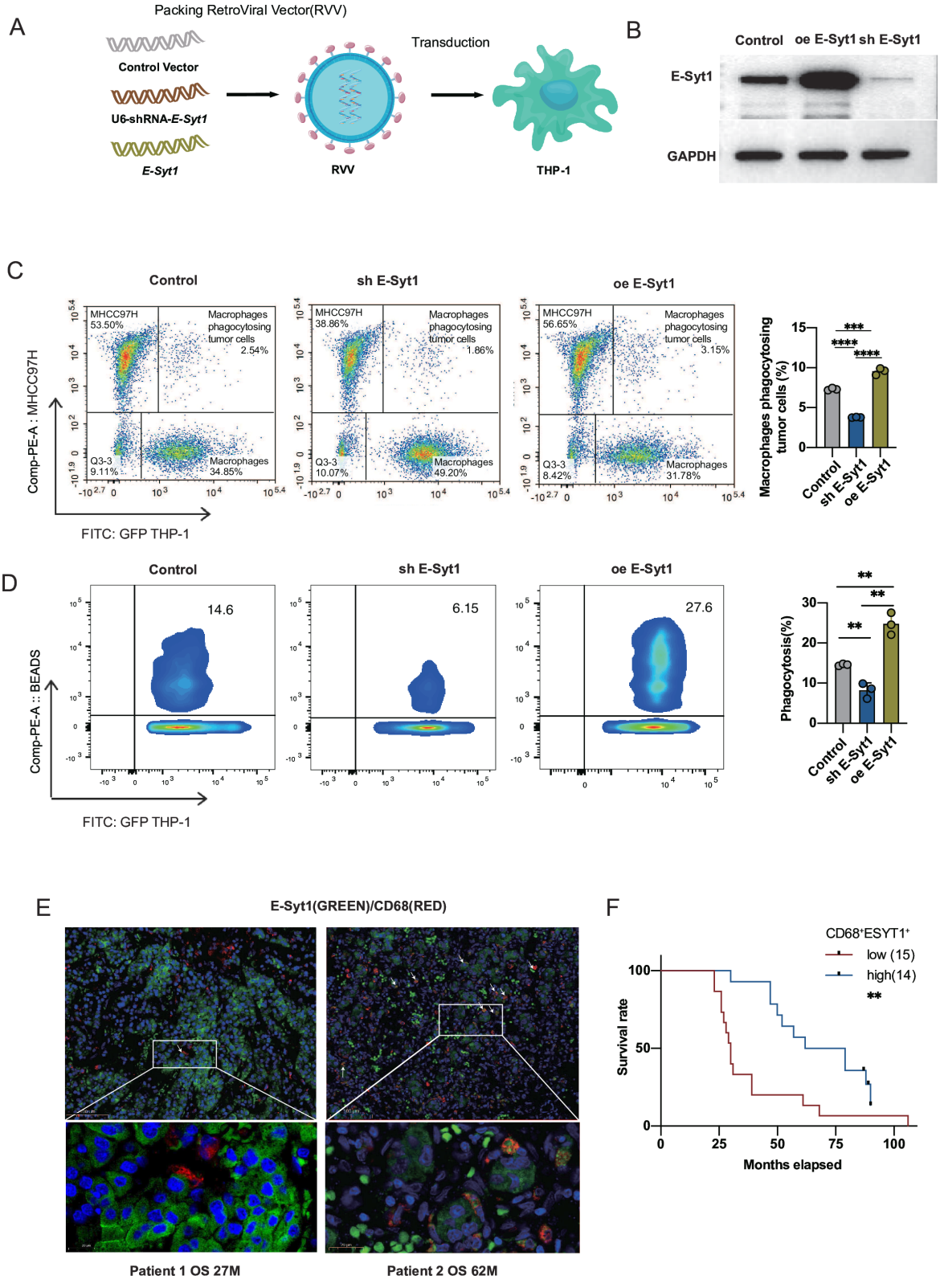

Figure 5 E-Syt1 promotes macrophage phagocytosis. (A) The image represents a schematic diagram of the construction of a retrovirus. (B) This western blot image illustrates the expression levels of E-Syt1 and GAPDH under three conditions: control, overexpressed E-Syt1 (oe E-Syt1) and knocked down E-Syt1 (sh E-Syt1). (C) Flow cytometry based phagocytosis of RFP-MHCC97H tumour cells by control, knocked down and overexpressed E-Syt1 in THP-1. Statistical significance was calculated with t-test pairwise comparisons among three groups of data comparisons, and data represent n=3 technical replicates. (D) The proportion of THP1 cells phagocytosing Red Zymosan in the three groups was detected and compared using flow cytometry. **p<0.01; ***p<0.001 from unpaired t-test, mean with SD. And data represent n=3 technical replicates. (E) Immunohistochemical staining was performed on human liver tumour tissues to detect CD68 and E-Syt1, with DAPI in blue, CD68 in red and E-Syt1 in green. Scale bar: 100 µm. (F) The 29 patients were divided into high and low groups based on the median number of CD68 and E-Syt1 double-positive cells, and overall survival time was compared between the two groups. The log-rank test was used in the overall survival analysis.

NLRP6 regulates phagocytosis by interacting with E-Syt1

In our previous result, we have demonstrated that Nlrp6 enhances macrophage phagocytosis and observed a negative correlation between Nlrp6 and E-Syt1, with evidence of their interaction. Additionally, we have confirmed that E-Syt1 promotes macrophage phagocytosis and that patients with higher E-Syt1 expression in macrophages exhibit longer survival. Based on these findings, we hypothesise that Nlrp6 may enhance macrophage phagocytosis through the regulation of E-Syt1. To test this hypothesis, we used retroviruses to construct stable shNlrp6-THP1 and oeNlrp6-THP1 cell lines. Subsequently, we co-transfected these cells with shRNA-E-Syt1 and oeRNA-E-Syt1 plasmids to generate four dual-transfected cell types: shNlrp6/oeE-Syt1, shNlrp6/shE-Syt1, oeNlrp6/shE-Syt1 and oeNlrp6/oeE-Syt1 (figure 6A). Following transfection, we will assess Nlrp6 and E-Syt1 protein expression to confirm successful protein editing (figure 6B). Next, we evaluated the phagocytic capacity of these four dual-transfected cell types, using THP-1 cells transfected with control viruses as the control group, measured as a percentage of phagocytosis. The results indicate that shNlrp6 cells exhibit significantly increased phagocytic capacity compared with the control group ($p<0.001$). However, there is no significant difference in phagocytic capacity between shNlrp6 and shNlrp6/oeE-Syt1 cells. In contrast, shNlrp6/shE-Syt1 cells show a significant reduction in phagocytic capacity compared with shNlrp6 cells ($p<0.0001$) (figure 6C), indicating that reduced E-Syt1 expression can reverse the enhanced phagocytic capacity induced by shNlrp6. This suggests that E-Syt1 functions downstream of Nlrp6 in regulating macrophage phagocytosis. Then we assessed the phagocytic capacities of control, oeNlrp6, oeNlrp6/shE-Syt1 and oeNlrp6/oeE-Syt1 cell lines. The data reveal that oeNlrp6 cells exhibit a significant reduction in phagocytic capacity compared with the control group ($p<0.001$). Furthermore, oeNlrp6/shE-Syt1 cells show a further decrease in phagocytic capacity compared with oeNlrp6 cells. In contrast, oeNlrp6/oeE-Syt1 cells exhibit a significant increase in phagocytic capacity compared with both oeNlrp6 and control cells ($p<0.001$) (figure 6D). These results suggest that overexpression of E-Syt1 can counteract the reduced phagocytic capacity induced by oeNlrp6, further supporting the notion that E-Syt1 functions downstream of Nlrp6 in regulating macrophage phagocytosis.

To further validate the upstream and downstream relationship between Nlrp6 and E-Syt1, we hypothesised that E-Syt1 functions downstream of Nlrp6 and controls the phagocytic capacity mediated by Nlrp6. The results indicate that shE-Syt1 cells show a significant reduction in phagocytic capacity compared with the control group. However, there is no significant difference in phagocytic capacity between shE-Syt1 and either oeNlrp6/shE-Syt1 or shE-Syt1/shNlrp6 cells (figure 6E). These findings suggest that when E-Syt1 expression is reduced, altering Nlrp6 levels does not affect phagocytic capacity. This supports the conclusion that E-Syt1 is downstream of Nlrp6 and is crucial for the regulation of phagocytosis by Nlrp6. Thus, E-Syt1 acts as the switch for Nlrp6-mediated changes in macrophage phagocytic activity.

And then we compared phagocytic capacity between oeE-Syt1 and shNlrp6/oeE-Syt1 and oeNlrp6/oeE-Syt1 cells. The results show that oeE-Syt1 and oeNlrp6/oeE-Syt1 cells exhibit a significant increase in phagocytic capacity compared with the control group. However, there is no significant difference in phagocytic capacity between oeE-Syt1 and oeNlrp6/oeE-Syt1 cells (figure 6F). This suggests that when E-Syt1 expression is overexpressed, altering Nlrp6 levels does not impact phagocytic capacity, further supporting the notion that E-Syt1 operates downstream of NLRP6. NLRP6 affects macrophage phagocytosis through the regulation of E-Syt1 expression.

In summary, E-Syt1 plays a pivotal role in the regulatory pathway by which NLRP6 modulates macrophage phagocytic capacity. NLRP6 influences phagocytosis through the regulation of E-Syt1, which acts as the downstream effector of NLRP6's regulatory effects.

The PYD segment of NLRP6 interacts with the SMP segment of E-Syt1

We have established that E-SYT1 acts as a pivotal regulator, modulating the influence of NLRP6 on macrophages. Building on this discovery, we sought to investigate the specific structural interaction between these two proteins, focusing on their domains.

E-SYT1 is an endoplasmic reticulum-localised, multidomain-containing protein that consists of a transmembrane (TM) domain, an Synaptotagmin-like Mitochondrial-lipid-binding Protein (SMP) domain and five C2 domains (C2A–C2E)[33] (figure 7A).

To identify which domain of E-SYT1 is responsible for binding to NLRP6, we generated a series of deletion mutants from the N terminus to the C terminus, tagged with Myc. These mutants included: Myc-E-SYT1-△TM (lacking the TM domain), Myc-E-SYT1-ΔTM+SMP (lacking both the TM and SMP domains) and Myc-E-SYT1-ΔC2 (lacking the C2 domains). Full-length (FL) E-SYT1 and these deletion mutants were individually transfected into HEK293T cells along with FLAG-tagged NLRP6. Our results showed that only FL E-SYT1 and E-SYT1-△TM, E-SYT1-△C2 domains bound to FLAG-tagged NLRP6, indicating that the SMP domain of E-SYT1 is necessary for its interaction with NLRP6 (online supplemental table 3)(figure 7C).

To further explore the structural basis of the interaction, we generated a series of deletion mutants from the N terminus to the C terminus, tagged with Flag. These mutants include: Flag-NLRP6-ΔPYD (lacking the PYD domain), Flag-NLRP6-ΔLRR (lacking the LRR domain) and Flag-NLRP6-ΔPYD+LRR (lacking both the PYD and LRR domains) (figure 7B). FL NLRP6 and these deletion mutants were individually transfected into HEK293T cells along with MYC-tagged E-SYT1. We observed that only FL NLRP6 and NLRP6-ΔLRR were able to bind to MYC-tagged E-SYT1, confirming that the PYD domain of NLRP6 is necessary for its interaction with E-SYT1 (figure 7D). The findings indicate that NLRP6 interacts with the SMP domain of E-SYT1 via its PYD domain, which in turn affects the function of E-SYT1 in macrophages (figure 7E).

DISCUSSION

This study investigates the role of NLRP6 in regulating macrophage function and its potential as a therapeutic target in HCC. NLRP6 deficiency significantly enhances macrophage phagocytosis through upregulation of E-Syt1, leading to the inhibition of HCC progression. We observed an abnormal elevation of NLRP6 expression in the patients with HCC, which correlates with the aggressive progression of the disease. This finding is consistent with previous research,[34] which indicated that $Nlrp6^{-/-}$ mice showed reduced HCC progression across multiple tumour models, further reinforcing the idea that NLRP6 plays a pivotal role in regulating tumour growth and immune cell activity in the liver.

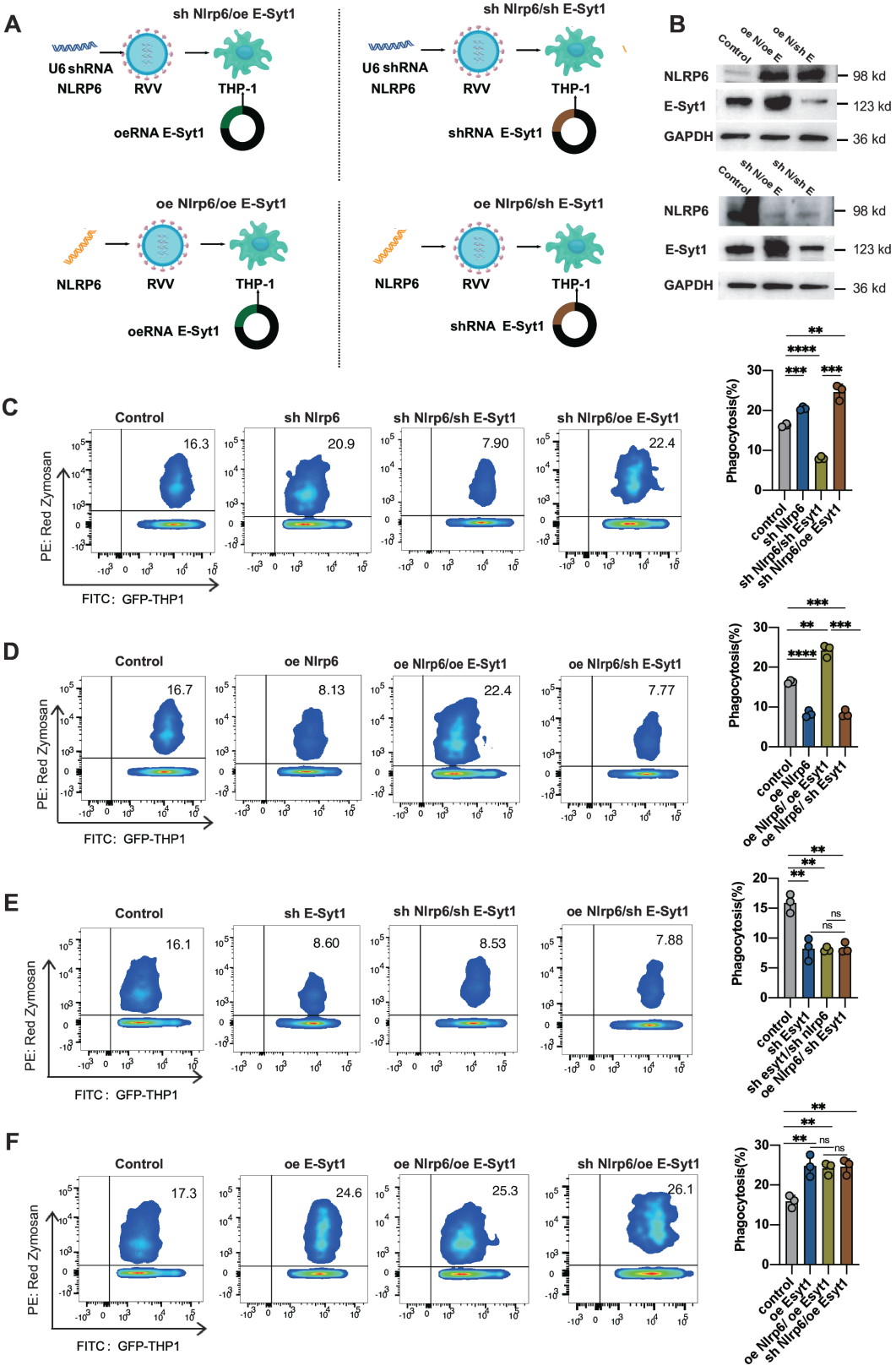

Figure 6 NLRP6 regulates phagocytosis by interacting with E-Syt1. (A) This schematic diagram represents two types of dual-transgenic macrophages, indicated by different treatments and genetic modifications. (B) This western blot image illustrates the expression levels of E-Syt1 and NLRP6 under two conditions: control, shE-Syt1/shNLRP6 and oeNLRP6/oeE-Syt1. (C–F) The proportion of THP1 cells phagocytosing Red Zymosan was assessed across various groups using flow cytometry, with bar charts showing phagocytic capacity as a percentage. (C) Comparison of control, shNLRP6, shNLRP6/shE-Syt1 and shNLRP6/oeE-Syt1 THP-1 cells. (D) Comparison of control, oeNLRP6, oeNLRP6/oeE-Syt1 and oeNLRP6/shE-Syt1 THP-1 cells. (E) Comparison of control, shE-Syt1, shE-Syt1/shNLRP6 THP-1 and oeNLRP6/shE-Syt1 cells. (F) Comparison of control, oeE-Syt1, oeNLRP6/oeE-Syt1 THP-1 cells and shNLRP6/oeE-Syt1. Statistical significance was determined using an unpaired t-test, mean with SD: **p<0.01, ***p<0.001, ****p<0.0001; 'ns' indicates no significant difference. NLRP6, NOD-like receptor family pyrin domain containing 6.

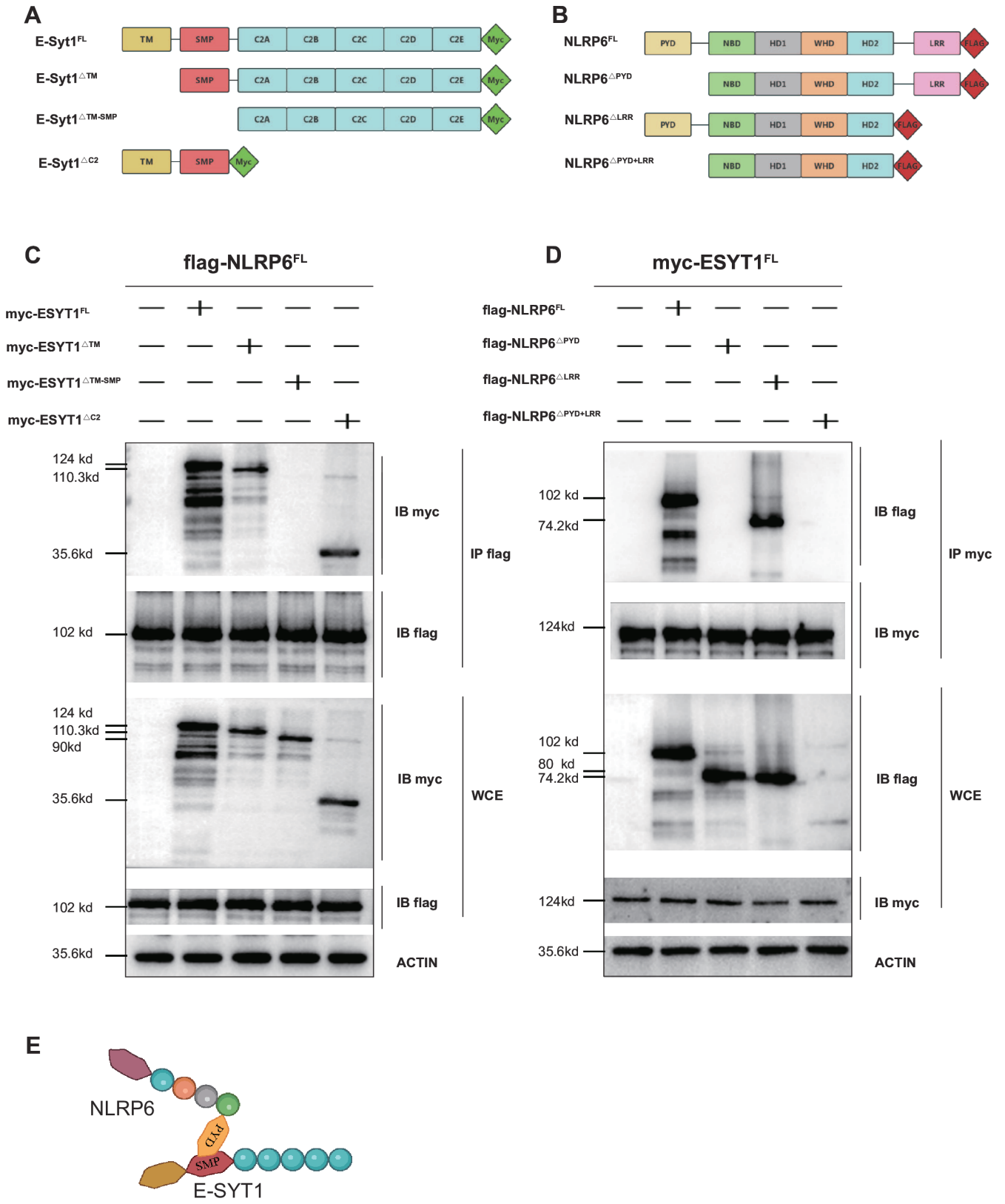

Figure 7 The PYD segment of NLRP6 interacts with the SMP segment of E-Syt1. (A) E-Syt1 domain structures: E-Syt1-FL: full-length E-Syt1. E-Syt1$^{\triangle TM}$: E-Syt1 lacking the transmembrane domain (TM). E-Syt1$^{\triangle TM+SMP}$: E-Syt1 lacks both the TM and SMP domains. E-Syt1$^{\triangle C2}$: E-Syt1 lacking the C2 domains. (B) NLRP6 domain structures. NLRP6^{FL}: full-length NLRP6. NLRP6$^{\triangle PYD}$: NLRP6 lacking the PYD domain. NLRP6$^{\Delta LRR}$: NLRP6 lacking the LRR domain. NLRP6$^{\triangle PYD+LRR}$: NLRP6 lacks both the PYD and LRR domains. (C) Immunoblot analysis of Myc immunoprecipitates of lysates of HEK293T cells transfected with FLAG-tagged NLRP6 and Myc-tagged full-length E-Syt1 (Myc-E-Syt1-FL) or E-Syt1 mutants E-Syt1$^{\triangle TM}$, E-Syt1$^{\triangle TM+SMP}$, E-Syt1$^{\triangle C2}$. (D) Immunoblot analysis of FLAG immunoprecipitates of lysates of HEK293T cells transfected with MYC-tagged E-Syt1 and FLAG-tagged full-length NLRP6 (FLAG-NLRP6-FL) or NLRP6 mutants NLRP6$^{\Delta PYD}$, NLRP6$^{\Delta LRR}$, NLRP6$^{\Delta PYD+LRR}$. (E) The diagram illustrating the combination of the SMP domain and the PYD domain. NLRP6, NOD-like receptor family pyrin domain containing 6.

One of the significant challenges in the field of cancer immunotherapy is the limited efficacy of macrophage-based therapies, particularly their reduced phagocytic function and inability to accumulate in sufficient numbers within the tumour microenvironment.[8] In this study, we address these two major limitations. We discovered that NLRP6 deficiency not only enhances macrophage infiltration into the liver but also significantly increases their phagocytic activity. These changes are directly correlated with reduced tumour progression, suggesting that NLRP6 deficiency can effectively boost macrophage-mediated tumour suppression. This discovery positions NLRP6 as a promising therapeutic target for enhancing macrophage-based therapies, potentially improving their tumour-killing capacity and their ability to accumulate within the tumour site.

At the mechanistic level, we identified that the PYD domain of NLRP6 interacts with the SMP domain of E-Syt1. This interaction was shown to regulate macrophage phagocytosis, as the absence of NLRP6 leads to an increase in E-Syt1 expression. E-Syt1, a protein known for its crucial role in endocytosis, modulates membrane curvature and tension, thus facilitating vesicle formation during phagocytosis. While the role of E-Syt1 in membrane dynamics during endocytosis has been well-established in various cell types, our study is the first to link this protein directly to macrophage phagocytosis,[28 35] providing novel insights into how NLRP6 and E-Syt1 cooperate in regulating immune responses. This finding introduces a new aspect of macrophage biology that could have important implications for both basic immunology and cancer therapy.

In addition to elucidating the molecular mechanisms, we also explored the therapeutic potential of targeting NLRP6 in clinical applications. Specifically, we tested the efficacy of Nlrp6$^{-/-}$ BMDMs in xenograft models and demonstrated that intratumoural injections of these NLRP6-deficient macrophages significantly inhibited tumour growth. This experiment highlights the therapeutic promise of incorporating NLRP6 inhibition into macrophages. By enhancing the phagocytic capacity and accumulation of macrophages, this strategy could potentially improve their tumour-killing capacity, offering a novel approach for macrophage-based immunotherapy in cancer treatment.

In conclusion, NLRP6 deficiency significantly enhances macrophage phagocytosis through upregulation of E-Syt1, leading to the inhibition of HCC progression. We identified that the PYD domain of NLRP6 interacts with the SMP domain of E-Syt1, providing insights into the molecular mechanism by which NLRP6 regulates macrophage function and tumour progression. These insights provide a foundation for developing personalised immunotherapies, where NLRP6 inhibition could be used to strengthen macrophage-based therapies, leading to more effective and targeted treatments for HCC and potentially other malignancies. The broader implications of this work offer promising directions for the future of cancer immunotherapy, paving the way for novel therapeutic strategies that can better harness the immune system's ability to fight cancer.

Acknowledgements This study was supported by grants from the National Natural Science Foundation of China, 82272956. We thank Shenzhen Cell Valley for providing retroviruses and plasmids, Professor YS for his revisions and suggestions, and Dr Grace Y Chen for providing Nlrp6−/− mice. We also appreciate the staff at the Peking University 302 Clinical Medical School for their care of the animals. We thank Dr Chunbao Zhou and Dr Huiwei Sun from the Central Laboratory for their assistance with flow cytometry. We would like to sincerely thank all the patients who generously provided their tissue samples for this study. Their participation and support have been invaluable in advancing our research. We also acknowledge their willingness to contribute to the study by allowing us to use their samples, and for trusting us to share the study results with them. Without their involvement, this research would not have been possible.

Contributors SL designed the study, conducted experiments, analyzed data, and wrote the manuscript. YL contributed to study design, experiments, and data analysis. YF, XJ, and ZL helped design experiments and interpret data. ZQ handled bioinformatic analysis. LY, GL, and TianyiZ collected clinical samples. TingZ and XZ performed experiments and data analysis. YS conceived the study, supervised the research, interpreted data, and co-wrote the manuscript. JH performed experiments. HZ and RS designed experiments and supervised the research. YL is the guarantor.

Funding This study was supported by grants from the National Natural Science Foundation of China, 82272956.

Competing interests None declared.

Patient and public involvement Patients and/or the public were not involved in the design, or conduct, or reporting, or dissemination plans of this research.

Patient consent for publication Not applicable.

Ethics approval This study involves human participants and was approved by Medical Ethics Committee of the 302nd Hospital of the PLAID: 2016002D. Participants gave informed consent to participate in the study before taking part.

Provenance and peer review Not commissioned; externally peer reviewed.

Data availability statement Data are available upon reasonable request.

ORCID iDs
Xiaodong Jia http://orcid.org/0000-0002-2145-6272
Tianyi Zhang http://orcid.org/0000-0001-9964-8840
Yinying Lu http://orcid.org/0000-0002-7737-2334

REFERENCES

1 Vogel A, Martinelli E, Vogel A, *et al*. Updated treatment recommendations for hepatocellular carcinoma (HCC) from the ESMO Clinical Practice Guidelines. *Ann Oncol* 2021;32:801–5.
2 Llovet JM, Castet F, Heikenwalder M, *et al*. Immunotherapies for hepatocellular carcinoma. *Nat Rev Clin Oncol* 2022;19:151–72.
3 Dal Bo M, De Mattia E, Baboci L, *et al*. New insights into the pharmacological, immunological, and CAR-T-cell approaches in the treatment of hepatocellular carcinoma. *Drug Resist Updat* 2020;51:100702.
4 Wan X, Wisskirchen K, Jin T, *et al*. Genetically-modified, redirected T cells target hepatitis B surface antigen-positive hepatocytes and hepatocellular carcinoma lesions in a clinical setting. *Korean J Hepatol* 2024;30:735.
5 Shin HE, Han J, Park JD, *et al*. Enhancing CAR-NK Cells Against Solid Tumors Through Chemical and Genetic Fortification with DOTAP-Functionalized Lipid Nanoparticles. *Adv Funct Materials* 2024;34:2315721.
6 Newick K, O'Brien S, Moon E, *et al*. CAR T Cell Therapy for Solid Tumors. *Annu Rev Med* 2017;68:139–52.
7 Brouillet A, Lafdil F. Risk factors of primary liver cancer initiation associated with tumour initiating cell emergence: novel targets for promising preventive therapies. *eGastroenterology* 2023;1:e100010.
8 Villanueva MT. Macrophages get a CAR. *Nat Rev Cancer* 2020;20:300.
9 Li N, Geng S, Dong Z-Z, *et al*. A new era of cancer immunotherapy: combining revolutionary technologies for enhanced CAR-M therapy. *Mol Cancer* 2024;23:117.
10 Klichinsky M, Ruella M, Shestova O, *et al*. Human chimeric antigen receptor macrophages for cancer immunotherapy. *Nat Biotechnol* 2020;38:947–53.
11 Guilliams M, Scott CL. Liver macrophages in health and disease. *Immunity* 2022;55:1515–29.
12 Cheng K, Cai N, Zhu J, *et al*. Tumor-associated macrophages in liver cancer: From mechanisms to therapy. *Cancer Commun* 2022;42:1112–40.
13 Guillot A, Tacke F. Spatial dimension of macrophage heterogeneity in liver diseases. *eGastroenterology* 2023;1:e000003.
14 Mantovani A, Allavena P, Marchesi F, *et al*. Macrophages as tools and targets in cancer therapy. *Nat Rev Drug Discov* 2022;21:799–820.

15 Cassetta L, Pollard JW. Targeting macrophages: therapeutic approaches in cancer. *Nat Rev Drug Discov* 2018;17:887–904.
16 Feng D, Guan Y, Wang Y, *et al*. Characterisation of macrophages in healthy and diseased livers in mice: identification of necrotic lesion-associated macrophages. *eGastroenterology* 2025;3:e100189.
17 Zucman-Rossi J, Villanueva A, Nault J-C, *et al*. Genetic Landscape and Biomarkers of Hepatocellular Carcinoma. *Gastroenterology* 2015;149:1226–39.
18 Yao F, Deng Y, Zhao Y, *et al*. A targetable LIFR-NF-κB-LCN2 axis controls liver tumorigenesis and vulnerability to ferroptosis. *Nat Commun* 2021;12:7333.
19 Lee SB. Periodontal manifestations of leukemia. *J Indiana Dent Assoc* 1986;65:23–4.
20 Lavin Y, Winter D, Blecher-Gonen R, *et al*. Tissue-resident macrophage enhancer landscapes are shaped by the local microenvironment. *Cell* 2014;159:1312–26.
21 Kim S-J, Feng D, Guillot A, *et al*. Adipocyte Death Preferentially Induces Liver Injury and Inflammation Through the Activation of Chemokine (C-C Motif) Receptor 2-Positive Macrophages and Lipolysis. *Hepatology* 2019;69:1965–82.
22 Rehg JE, Bush D, Ward JM. The utility of immunohistochemistry for the identification of hematopoietic and lymphoid cells in normal tissues and interpretation of proliferative and inflammatory lesions of mice and rats. *Toxicol Pathol* 2012;40:345–74.
23 Guillot A, Kohlhepp MS, Bruneau A, *et al*. Deciphering the Immune Microenvironment on A Single Archival Formalin-Fixed Paraffin-Embedded Tissue Section by An Immediately Implementable Multiplex Fluorescence Immunostaining Protocol. *Cancers (Basel)* 2020;12:2449.
24 Guillot A, Buch C, Jourdan T. Kupffer Cell and Monocyte-Derived Macrophage Identification by Immunofluorescence on Formalin-Fixed, Paraffin-Embedded (FFPE) Mouse Liver Sections. *Methods Mol Biol* 2020;2164:45–53.
25 Mackowiak B, Fu Y, Maccioni L, *et al*. Alcohol-associated liver disease. *J Clin Invest* 2024;134:e176345.
26 Yao J, Kwon SE, Gaffaney JD, *et al*. Uncoupling the roles of synaptotagmin I during endo- and exocytosis of synaptic vesicles. *Nat Neurosci* 2011;15:243–9.
27 Zhang M, Li X, Zhuo S, *et al*. Enriched Environment Enhances Sociability Through the Promotion of ESyt1-Related Synaptic Formation in the Medial Prefrontal Cortex. *Mol Neurobiol* 2024;61:3019–30.
28 Yu H, Liu Y, Gulbranson DR, *et al*. Extended synaptotagmins are Ca2+-dependent lipid transfer proteins at membrane contact sites. *Proc Natl Acad Sci U S A* 2016;113:4362–7.
29 Reticulum SYE. Endoplasmic reticulum – plasma membrane crosstalk mediated by the extended synaptotagmins. In: Tagaya M, Simmen T, eds. *Organelle contact sites: from molecular mechanism to disease*. Singapore: Springer, 2017: 83–93. Available: https://doi.org/10.1007/978-981-10-4567-7_6
30 Giordano F, Saheki Y, Idevall-Hagren O, *et al*. PI(4,5)P2-Dependent and Ca2+-Regulated ER-PM Interactions Mediated by the Extended Synaptotagmins. *Cell* 2013;153:1494–509.
31 Janer A, Morris JL, Krols M, *et al*. ESYT1 tethers the endoplasmic reticulum to mitochondria and is required for mitochondrial lipid and calcium homeostasis. *Cell Biology* [Preprint].
32 Saheki Y, De Camilli P. Endoplasmic Reticulum-Plasma Membrane Contact Sites. *Annu Rev Biochem* 2017;86:659–84.
33 Herdman C, Moss T. Extended-Synaptotagmins (E-Syts); the extended story. *Pharmacol Res* 2016;107:48–56.
34 Chang L, Xu L, Tian Y, *et al*. NLRP6 deficiency suppresses colorectal cancer liver metastasis growth by modulating M-MDSC-induced immunosuppressive microenvironment. *Biochim Biophys Acta Mol Basis Dis* 2024;1870:167035.
35 Sahay G, Alakhova DY, Kabanov AV. Endocytosis of nanomedicines. *J Control Release* 2010;145:182–95.